Physical Chemistry Chemical Physics

c3cp51651b

High performance PbS Quantum Dot Sensitized Solar Cells exceeding 4% efficiency: the role of metal precursors in the electron injection and charge separation

Q1
Q2

Victoria González-Pedro, Cornelia Sima, Gabriela Marzari, Pablo P. Boix, Sixto Giménez, Qing Shen, Thomas Dittrich and Iván Mora-Seró*

Here we report the preparation of high performance Quantum Dot Solar Cells (QDSCs) based on PbS–CdS co-sensitized nanoporous TiO$_2$ electrodes.

Q3

Please check this proof carefully. **Our staff will not read it in detail after you have returned it.**

Translation errors between word-processor files and typesetting systems can occur so the whole proof needs to be read. Please pay particular attention to: tabulated material; equations; numerical data; figures and graphics; and references. If you have not already indicated the corresponding author(s) please mark their name(s) with an asterisk. Please e-mail a list of corrections or the PDF with electronic notes attached – do not change the text within the PDF file or send a revised manuscript. Corrections at this stage should be minor and not involve extensive changes. All corrections must be sent at the same time.

Please bear in mind that minor layout improvements, e.g. in line breaking, table widths and graphic placement, are routinely applied to the final version.

Please note that, in the typefaces we use, an italic vee looks like this: v, and a Greek nu looks like this: ν.

We will publish articles on the web as soon as possible after receiving your corrections; **no late corrections will be made.**

Please return your **final** corrections, where possible within **48 hours** of receipt, by e-mail to: pccp@rsc.org

Queries for the attention of the authors

Editor's queries are marked on your proof like this Q1, Q2, etc. and for your convenience line numbers are indicated like this 5, 10, 15, …

Please ensure that all queries are answered when returning your proof corrections so that publication of your article is not delayed.

Query reference	Query	Remarks
Q1	For your information: You can cite this article before you receive notification of the page numbers by using the following format: (authors), Phys. Chem. Chem. Phys., (year), DOI: 10.1039/c3cp51651b.	
Q2	Please carefully check the spelling of all author names. This is important for the correct indexing and future citation of your article. No late corrections can be made.	
Q3	Please check that the inserted GA text is suitable.	
Q4	In the sentence beginning 'Here we report the…' should 'Quantum Dot Solar Cells' be changed to 'Quantum Dot Sensitized Solar Cells'?	
Q5	In the sentence beginning 'A 0.02 M methanolic…', a phrase appears to be missing after '0.02 M methanolic solution' and '0.05 M methanolic solution'. Please check this carefully and indicate any changes required here.	
Q6	The sentence beginning ''An unprecedented efficiency…'' has been altered for clarity, please check that the meaning is correct.	
Q7	Ref. 13: Please provide: page number(s).	
Q8	Ref. 15: Please provide initial(s) for the sixth author.	
Q9	Ref. 45: Please provide initial(s) for the first author.	

PCCP

PAPER

High performance PbS Quantum Dot Sensitized Solar Cells exceeding 4% efficiency: the role of metal precursors in the electron injection and charge separation†

Victoria González-Pedro,[a] Cornelia Sima,[abc] Gabriela Marzari,[a] Pablo P. Boix,[a] Sixto Giménez,[a] Qing Shen,[de] Thomas Dittrich[f] and Iván Mora-Seró*[a]

Here we report the preparation of high performance Quantum Dot Solar Cells (QDSCs) based on PbS–CdS co-sensitized nanoporous TiO$_2$ electrodes. QDs were directly grown on the TiO$_2$ mesostructure by the Successive Ionic Layer Absorption and Reaction (SILAR) technique. This method is characterized by a fast deposition rate which involves random crystal growth and poor control of the defect states and lattice mismatch in the QDs limiting the quality of the electrodes for photovoltaic applications. In this work we demonstrate that the nature of the metallic precursor selected for SILAR has an active role in both the QD's deposition rate and the defect's distribution in the material, with important consequences for the final photovoltaic performance of the device. For this purpose, acetate and nitrate salts were selected as metallic precursors for the SILAR deposition and films with similar absorption properties and consequently with similar density of photogenerated carriers were studied. Under these conditions, ultrafast carrier dynamics and surface photovoltage spectroscopy reveal that the use of acetate precursors leads to higher injection efficiency and lower internal recombination due to contribution from defect states. This was corroborated in a complete cell configuration with films sensitized with acetate precursors, achieving unprecedented photocurrents of ∼22 mA cm^{-2} and high power conversion efficiency exceeding 4%, under full 1 sun illumination.

Introduction

Since the early nineties, sensitized solar cells[1] have attracted a great deal of attention as a low cost alternative to photovoltaic devices. Over the last two decades, intensive effort has been made around the world in order to increase the efficiencies of

these devices with a current record efficiency of 12%.[2] In spite of this remarkable performance, there is still room for further improvement. One of the strategies to improve the efficiency of these devices entails shifting the light absorption threshold into the near IR region, where the solar photon flux density is maximum. Inorganic semiconductor materials appear to be ideal candidates as sensitizers, operating in the near IR region, since the bulk band gap of some of these semiconductors (such as PbS) perfectly matches the spectral range of interest for light harvesting.

In the last few years, the use of inorganic semiconductors as alternative sensitizers for Dye Sensitized Solar Cells (DSCs) has experienced an impressive enhancement,[3–9] reflected in the continuous growth of the number of scientific papers published. The efficiencies obtained with these sensitizers remain below those reported for molecular dyes. However, the extremely easy preparation based on solution chemistry and the high potentiality (high extinction coefficient,[10] tunable band gap in the quantum confinement regime,[11] and large intrinsic dipole moment[12]) of these systems have boosted the research

[a] Photovoltaic and Optoelectronic Devices Group, Departament de Física, Universitat Jaume I, 12071 Castelló, Spain. E-mail: sero@fca.uji.es
[b] University of Bucharest, Faculty of Physics, 405 Atomistilor, P.O. Box MG-11, 077125, Bucharest-Magurele, Romania
[c] National Institute of Lasers, Plasma and Radiation Physics, Atomistilor 409 street, P.O. Box MG 36, Bucharest-Magurele, 077125, Romania
[d] Department of Engineering Science, Faculty of Informatics and Engineering, The University of Electro-Communications, 1-5-1 Chofugaoka, Chofu, Tokyo 182-8585, Japan
[e] PRESTO, Japan Science and Technology Agency (JST), 4-1-8 Honcho, Kawaguchi, Saitama 332-0012, Japan
[f] Helmholtz-Zentrum Berlin für Materialien und Energie GmbH, Glienicker Strasse 100, 14109 Berlin, Germany
† Electronic supplementary information (ESI) available. See DOI: 10.1039/c3cp51651b

This journal is © the Owner Societies 2013

Phys. Chem. Chem. Phys., 2013, **00**, 1–9 | 1

in this field.[3–9] The recent reports of perovskite semiconductors on a nanoporous matrix with outstanding efficiencies, around 10%,[13,14] will undoubtedly enhance the interest in inorganic semiconductors as light harvesting materials in nanostructured devices.

One of the fundamental differences between inorganic semiconductors and dyes lies in the synthetic versatility of the former ones. Inorganic semiconductors can be prepared by following many different synthetic routes and the growth method has a significant influence on their properties.[15,16] As an example, colloidal chemistry offers a precise control over the crystalline properties and size of the semiconductor material.[11] Below a critical size, these materials exhibit quantum confinement effects with the band gap controlled by particle size. The solar cells using these materials as sensitizers are termed Quantum Dot Sensitized Solar Cells (QDSCs). Colloidal QDs can be directly attached to the nanoporous structure of a sensitized solar cell[17–19] or using a bi-functional linker.[18,20,21] Unfortunately, the QD loading of sensitized electrodes with colloidal QDs was generally shown to be insufficient to harvest all the incident light.[15] However, the photovoltaic efficiency of solar cells with colloidal QDs is significantly enhanced when inverted type-I CdS/CdSe core–shell QDs are employed.[22] In order to increase QD loading, *in situ* growth of the inorganic semiconductor on a nanostructured photoanode can be carried out by low cost solution techniques such as Chemical Bath Deposition (CBD)[16,23–25] or Successive Ionic Layer Absorption and Reaction (SILAR).[26–28] The advantage of higher QD loading is partially balanced by the lower control over the QD growth conditions. Compared to colloidal QDs, lower crystalline quality is obtained for QDs directly grown on nanostructured electrodes with a broad distribution of QD sizes together with the development of grain boundaries.[15] Under these conditions, it is expected that the growth method and growth conditions dramatically affect the final photovoltaic performance when directly grown QDs are employed. It has been shown that CdS/CdSe QDSCs grown by CBD systematically exhibit higher open circuit voltage, V_{oc}, compared to QDs grown by SILAR.[16] Here we show that the selection of the metallic precursors to grow PbS–CdS QDs by SILAR has a dramatic effect on the final QDSC performance.

PbS is a particularly interesting semiconductor material, with a bulk band gap in the IR region, 0.41 eV.[29] Its band gap can be tuned by reducing the size of the PbS nanoparticles to the quantum confinement region. By tuning the band gap of PbS, a double objective can be attained: (i) better match with the optimum absorption band gap[30] and (ii) a correct band alignment in order to inject photoexcited electrons into the TiO$_2$ conduction band (CB).[31] With a band gap in the near IR region, it is expected that PbS QDSCs exhibit high photocurrents, J_{sc}, larger than 20 mA cm^{-2}, as it has been observed with PbS colloidal QDs in thin film colloidal QD solar cells (Schottky[32] and Depleted Heterojunction Solar cells[33]). However, these high current densities have not been obtained in the case of QDSCs until the present study where we report a photocurrent as high as 22.3 mA cm^{-2}. In order to attain high photocurrent with PbS QDSCs some important obstacles

needed to be overcome. The most important one relied on the solar cell stability, since PbS is not stable in contact with polyionide or polysulfide electrolytes.[34] We solved this problem by coating PbS with CdS, obtaining a stable behavior of the heterostructured PbS–CdS absorber with a polysulfide electrolyte.[35,36] On the other hand, other authors have shown that the nanostructured electrode for PbS–CdS QDSCs is not fully optimized. The group of Qing Wang showed that it is possible to increase PbS–CdS photocurrents, up to 17.4 mA cm^{-2}, by using nanostructured SnO$_2$ instead of TiO$_2$.[37] Alternatively, Qingbo Meng's group showed that a hierarchical pore distribution of the TiO$_2$ nanostructured photoanode led to a significant increase of the solar cell performance, J_{sc} = 18.8 mA cm^{-2} and efficiency η = 3.82%.[38] Here we show that further improvement, J_{sc} = 22.3 mA cm^{-2} and η = 4.20%, can be obtained by optimizing the crystal growth of PbS–CdS, using different precursor salts. We have systematically analyzed the prepared samples to unveil the physical origin of the increase of efficiency. Compared to electrodes sensitized with nitrate precursors, those sensitized with acetate precursors exhibit higher injection rate (from the sensitizer to TiO$_2$) and consequently lower internal recombination due to a different contribution of the QD surface states.

Experimental section

Device preparation

The photoelectrodes were prepared using a double layer film of interconnected titania nanoparticles deposited over FTO glass (Pilkington, ∼15 Ω sq^{-1} resistance) by doctor blade. The mesoporous film consists of a 9 μm-thick transparent layer of TiO$_2$ (DSL 18-NRT, 20 nm average particle size) and a 5 μm-thick layer of scattering particles (DSL, WERO-4, 300–400 nm particle size distribution). The films were sintered for 30 minutes at 450 °C to obtain a good electrical contact between nanoparticles and the film thickness was measured by profilometry (Dektak 6 from Veeco). The FTO glass was previously coated by a compact layer of 150 nm TiO$_2$ deposited by spray pyrolysis of titanium(IV)bis(acetoacetonato) di(isopropanoxylate) and sintered at 450 °C for 30 minutes.

The Successive Ionic Layer Adsorption and Reaction (SILAR) technique was used to grow double layer PbS–CdS films. This technique, well described in previous works,[26,28,36] involves the crystal growth "layer by layer" by sequentially dipping the substrates into the ionic precursor solutions for 1 min. A 0.02 M methanolic solution was used as a lead source for PbS deposition and a 0.05 M methanolic solution as a cadmium precursor for CdS. The sulfide precursors were 0.02 M and 0.05 M solutions of Na$_2$S·9H$_2$O in methanol–water (1 : 1, v/v) for Pb^{2+} and Cd^{2+} ions, respectively. After the each dipping step in a precursor solution, the electrodes were dipped in a solution without the precursor in order to rinse the excess of precursor. The sequence of dipping processes metallic precursor–rinse–sulphur precursor–rinse constitutes a SILAR cycle. The amount of deposited material increases with the number of SILAR cycles. Two types of precursors for Cd and Pb were employed,

2 | *Phys. Chem. Chem. Phys.,* 2013, **00**, 1–9

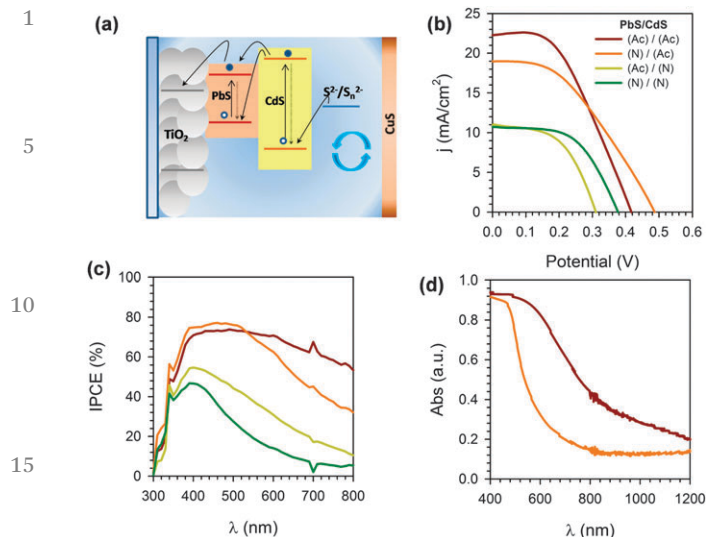This journal is © the Owner Societies 2013

Fig. 1 (a) Schematic diagram of the PbS–CdS sensitized solar cells. Solid arrows indicate electron photoexcitation and injection, and dotted arrows internal recombination (before injection), blue arrows indicate the regenerative reaction of QDs with the redox couple and the reverse reaction at the counter electrode. (b) Current–voltage curves under 1 sun illumination and (c) IPCE of the analyzed devices. QDs were *in situ* grown by a SILAR technique with 2 cycles for PbS and 5 cycles for CdS. (Ac) and (N) in the legend refers to the metallic salt source employed for PbS and CdS deposition by the SILAR process, acetate and nitrate, respectively. (d) Absorption spectra of electrodes produced with CdS grown with cadmium acetate salt as a cadmium precursor. Identical color code is used in (b)–(d).

CH_3COO^- (acetate, hereafter Ac) and NO_3^- (nitrate, hereafter N) salts. High magnification TEM pictures of the electrodes sensitized with different precursors are compiled as S1 (ESI†). In all the experiments, the SILAR process was carried out using SILAR equipment from ISTest at room temperature under an air atmosphere. After sensitization, all the samples analyzed in this study were coated with 2 SILAR cycles of ZnS, by alternately dipping into 0.1 M $Zn(CH_3COO)_2$ and 0.1 M $Na_2S \cdot 9H_2O$ solutions at a rate of 1 min per dip and rinsing with Milli-Q ultrapure water between dips.

The device preparation was carried out by sandwiching the working electrode (sensitized photoanode) with the Cu_2S counter electrode and using the polysulfide electrolyte and scotch tape as a spacer (50 μm thick). The polysulfide electrolyte was 1 M Na_2S, 1 M S, and 0.1 M NaOH solution in Milli-Q ultrapure water under a nitrogen bubbling mixture and the Cu_2S counter electrodes were prepared by immersing brass in HCl solution at 70 °C for 5 min and subsequently dipping into polysulfide solution for 1 min, resulting in a porous Cu_2S electrode.[39] The geometric area of the cells was 0.196 cm². In Fig. 1(a) a cartoon of the analyzed QDSC structure is depicted.

For each studied device configuration, at least two identical cells, but generally more, have been produced in order to check the reproducibility of the analyzed devices. The dispersion is lower than 15%. Some examples of reproducibility are shown in S2 (ESI†).

Characterization of TiO₂ sensitized electrodes

The absorption spectra were recorded using a Cary 500 UV-VIS Varian photospectrometer. TEM measurements were carried out using a JEM-2100 Electron Microscope (JEOL) operated at 200 kV.

Photoelectrochemical characterization

The Incident Photon to Current Efficiency (IPCE) measurements were performed employing a 150 W Xe lamp coupled with a monochromator controlled by a computer; the photocurrent was measured using an optical power meter 70310 from Oriel Instruments, using a Si photodiode to calibrate the system. Current potential (J–V) curves and impedance spectroscopy (IS) measurements were obtained using a FRA equipped PGSTAT-30 from Autolab. The cells were illuminated using a solar simulator Sun2000 from ABET Technologies at AM 1.5 G, where the light intensity was adjusted using an NREL-calibrated Si solar cell with a KG-5 filter to 1 sun intensity (100 mW cm⁻²). J–V curves under illumination were obtained using a mask and with no antireflective layer. Impedance spectroscopy measurements were carried out under dark conditions at different forward biases, by applying a 20 mV AC sinusoidal signal over the constant applied bias with the frequency ranging between 400 kHz and 0.1 Hz.

Ultrafast characterization

The principle and setup of the lens-free heterodyne detection transient grating (LF-HD-TG) technique have been reported in detail in previous papers.[40,41] In this experiment, the laser source was a titanium/sapphire laser (CPA-2010, Clark-MXR Inc.) with a wavelength of 775 nm, a repetition rate of 1 kHz, and a pulse width of 150 fs. The light was separated into two beams. One of them was used as a probe pulse. The other light beam was used to pump an optical parametric amplifier (OPA) (a TOAPS from Quantronix) to generate light pulses with a wavelength tunable from 290 nm to 3 μm. It was used as a pump light in the TG measurement. In this study, the pump pulse wavelength was 520 nm and the probe pulse wavelength was 775 nm.

Surface photovoltage spectroscopy (SPV)

For recording SPV spectra the measurements were performed in parallel-plate capacitor arrangement.[42] SPV spectra were measured under high vacuum by using a halogen lamp with a quartz-prism monochromator for the excitation and a chopper for modulation (modulation frequency 8 Hz, signal detected using a lock-in amplifier). For the time-resolved and surface photovoltage spectroscopy 4 μm-thick, nanocrystalline transparent TiO₂ thin films were prepared, without a scattering layer.

Results and discussion

Combining Pb and Cd, nitrate and acetate salts, four different combinations of PbS–CdS solar cells can be produced. Fig. 1 shows the results obtained with sensitized electrodes produced after 2 and 5 cycles of PbS and CdS, respectively. The number of SILAR cycles has been optimized after a preliminary study on the solar cell performance with the number of SILAR cycles and the metallic precursor, see S3 and S4 (ESI†). The solar cell performance, Fig. 1(b), is clearly affected by the metallic

This journal is © the Owner Societies 2013

Phys. Chem. Chem. Phys., 2013, **00**, 1–9 | **3**

Table 1 Photovoltaic parameters of the analyzed sensitized solar cells under 1 sun illumination (short circuit current, J_{sc}; photovoltage, V_{oc}; fill factor, FF; and conversion efficiency, η). Photoanodes were sensitized by SILAR using 2 cycles for PbS and 5 cycles for CdS

Sample	J_{sc} (mA cm^{-2})	V_{oc} (V)	FF	η (%)
Pb(Ac)–Cd(Ac)	22.28	0.416	0.453	4.20
Pb(N)Cd(Ac)	18.98	0.485	0.415	3.82
Pb(Ac)Cd(N)	11.26	0.318	0.513	1.80
Pb(N)–Cd(N)	10.86	0.361	0.548	2.20

precursor employed for the growth of both PbS and CdS. The solar cell parameters extracted from the J–V curves plotted in Fig. 1(b) are shown in Table 1. The enhancement in solar cell performance is particularly dramatic when Cd(Ac) is used as a cadmium precursor, leading to a remarkable photocurrent, with values higher than 20 mA cm^{-2} when Pb(Ac) is also employed as a lead precursor. An unprecedented efficiency of 4.20% was obtained for the cell using acetate precursors for both materials. A similar efficiency, 4.24%, but with lower photocurrent values has been observed when only one SILAR cycle with Pb(Ac) was applied, see S4 (ESI†). This extraordinarily high photocurrent can be reproducibly obtained, see S2 (ESI†). These large photocurrents are due to the extension of the light absorption to the red and near IR (NIR) obtained with the PbS sensitization, as evidenced by the IPCE spectra shown in Fig. 1(c).

The IPCE spectra shown in Fig. 1(c) clearly reflect that with an identical number of SILAR cycles, the use of the acetate (Ac) precursor for Cd or Pb deposition systematically leads to higher external quantum efficiency compared to the (N) precursor. Fig. 1(d) shows the absorbance of sensitized electrodes with the Cd (Ac) precursor and the two different Pb precursors. It is clear that the use of the acetate precursor enhances light absorption when the rest of the synthetic parameters (the number of SILAR cycles, dipping time, solution concentration) are kept constant. The use of acetate precursors increases the PbS and CdS deposition rate and consequently the amount of deposited material, see also S3 (ESI†).

In a previous study, we showed that fluorine treatment of the bare TiO$_2$ electrode also enhances the PbS deposition kinetics.[35] Basically, the photocurrent was enhanced due to a higher amount of deposited PbS, when the fluorine treatment was applied to TiO$_2$. However, the recombination rate in PbS–CdS QDSCs increases with the amount of PbS deposited material,[36] and a judicious balance between photocurrent and photovoltage is compulsory to optimize the conversion efficiency. In order to further investigate the role of the metallic precursor in PbS–CdS QDSCs, solar cells with electrodes sensitized by a different number of SILAR cycles but the same amount of deposited material, see Fig. 2(a), were prepared. The corresponding J–V curves are plotted in Fig. 2(b) and the photovoltaic parameters of these devices are summarized in Table 2. Higher J_{sc} is obtained for the cell prepared using the Pb(Ac) precursor, suggesting an additional role of the precursor material in the final cell performance besides the change in the deposition rate.
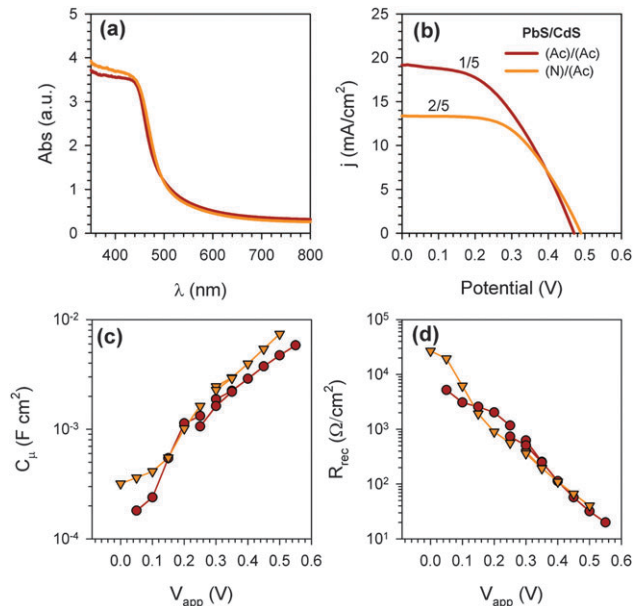

Fig. 2 Study of the role of the PbS salt precursor. PbS–CdS samples were prepared using acetate and nitrate as lead sources varying the SILAR conditions to obtain films with comparable absorption properties. The notation (X/Y) is referred to the number of SILAR cycles for PbS (X) and CdS (Y), respectively. (a) Absorption spectra, (b) J–V curves, (c) chemical capacitance, C_μ, and (d) recombination resistance, R_{rec}, as a function of applied voltage, V_{app}.

In order to unveil the origin of this enhanced performance with acetate precursors, cells plotted in Fig. 2(a) and (b) have been characterized by impedance spectroscopy and analyzed with the standard models for QDSCs.[18,28,36,43,44] The compared values obtained for chemical capacitance, C_μ, and recombination resistance, R_{rec}, are depicted in Fig. 2(c) and (d), respectively. The similar values obtained for C_μ indicate that the nature of the precursor does not affect the position of the TiO$_2$ conduction band.[44] Additionally, the recombination resistance, R_{rec}, is very similar for both precursors, Fig. 2(d). This result suggests that there is no change in the recombination rate of electrons in the TiO$_2$ with acceptor species in the QDs and/or the electrolyte, since these are the recombination processes susceptible to be monitored by IS.[44,45] Moreover, this result is in good agreement with the similar V_{oc} obtained for both cells (Fig. 2b and Table 2). Consequently, both solar cells are similar in terms of light absorption and IS characterization, although their photovoltaic behavior is clearly different, particularly in terms of J_{sc}. This means that the origin of the difference relies on a process which is not accessible by these techniques: electron/hole photoinjection after photocarrier generation.

Table 2 Photovoltaic parameters of the solar cells plotted in Fig. 2 under 1 sun illumination

Sample (PbS–CdS)	No. SILAR cycles (PbS–CdS)	J_{sc} (mA cm^{-2})	V_{oc} (V)	FF	η (%)
(Ac)/(Ac)	1/5	19.5893	0.471	0.449	4.15
(N)/(Ac)	2/5	13.3645	0.488	0.543	3.55

4 | *Phys. Chem. Chem. Phys.*, 2013, **00**, 1–9
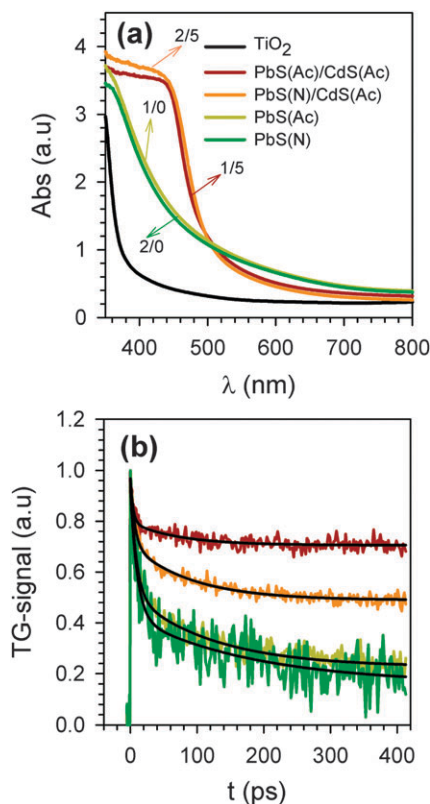
This journal is © the Owner Societies 2013

Fig. 3 (a) Absorption spectra for Pb–CdS co-sensitized and PbS single sensitized TiO$_2$ photoanodes employing acetate (Ac) and nitrate (N) as lead precursors for PbS growth, while only (Ac) precursor was used for CdS growth. (X/Y) is referred to the number of SILAR cycles for PbS (X) and CdS (Y), respectively. (b) TG responses measured under N$_2$ of the electrodes plotted in (a), solid line is the result of the fitting using eqn (2).

Ultrafast processes, as photoinjection, have been characterized by the transient grating (TG) technique.[40,41] In parallel with the experiments presented in Fig. 2, we prepared samples for ultrafast characterization with the same optical density, Fig. 3(a). From the absorption spectra for both sets of samples we can assume that films have similar density of generated photocarriers.

Fig. 3(b) shows the TG response of the electrodes characterized in Fig. 3(a) measured under a N$_2$ atmosphere. The experiments were carried out with a pump pulse wavelength of 520 nm and the probe pulse wavelength of 775 nm. At this excitation wavelength, the optical absorption of the anatase TiO$_2$ electrode and the CdS shell is negligible in comparison with the absorption from PbS. Consequently, the TG signals can be ascribed to the optical absorption of the PbS QDs, see Fig. 3(a). This excitation allows monitoring the effects of the CdS coating on the carrier dynamics of PbS QDs. The TG signal of the semiconductor QDs on the fast time scale used in this study (less than ns) is proportional to the change in the refractive index, $\Delta n(t)$, of the sample due to photoexcitation, which can be approximately determined by[40,41]

$$\Delta n(t) = A \left(\frac{N_e(t)}{m_e} + \frac{N_h(t)}{m_h} \right) \tag{1}$$

where the first and second term represent the changes in refractive index induced by photoexcited electrons and holes, respectively. $N_e(t)$ and $N_h(t)$ are the photoexcited electron and hole densities, respectively. m_e and m_h are the effective masses of electrons and holes, respectively, and A is a proportionality constant. The exact contribution of electrons and holes to $\Delta n(t)$ depends inversely on their effective mass. According to the Drude theory, we can consider that only free photoexcited electrons and holes are responsible for the population grating signals. For bulk PbS, the effective masses of electrons and holes are $0.09m_0$ and $0.09m_0$ (m_0 is the electron rest mass),[46] respectively, so both the photoexcited electron and hole carrier densities in the PbS QDs contribute to the signal and it is not possible to discriminate the origin between electrons and holes. It is known that the effective mass of electrons for TiO$_2$ is about $30m_0$, which is about three orders larger than that for PbS. Therefore, the TG signal due to the injected electrons in TiO$_2$ can be ignored.

We found that the TG response for PbS and PbS–CdS sensitized electrodes can be accurately fitted with a double exponential decay plus an offset, as shown in eqn (2),

$$TG = A_1 e^{\frac{-t}{\tau_1}} + A_2 e^{\frac{-t}{\tau_2}} + A_3 \tag{2}$$

where A_1, A_2 and A_3 are constants, and τ_1 and τ_2 are the time constants of the two decay processes. The fitting curves obtained using eqn (2) are represented as solid black lines in Fig. 3(b) and the values obtained from the fitting are indicated in Table 3. Here, the constant term A_3 corresponds to the slowest decay process, in which the decay time (in the order of ns) is much longer compared to the time scale of 400 ps measured in the present study. The three different decay processes have a weight on the total decay process defined as $A_i/(A_1 + A_2 + A_3)$, where $i = 1, 2$ and 3 is the process that is weighted. The obtained weights for the different processes are also indicated in Table 3.

The dependence of the TG response on the pump intensity was measured and it was found that the dependence of the maximum signal intensity on the pump intensity was linear. Additionally, the waveforms of the different responses perfectly overlapped when they were normalized. These results indicate that the time constants were independent of the pump intensity, and many-body recombination processes such as Auger recombination could be neglected. Therefore, it is reasonable to assume that the decay processes of photoexcited electrons and holes in the PbS QDs are due to one-body recombination processes such as trapping and/or transfer. As shown in Table 3, the decay times τ_1 and τ_2 of the two fast decay processes are about few ps and a few tens to hundreds ps, respectively. τ_1 and τ_2 decrease as PbS(N) > PbS(Ac) > PbS(N)–CdS(Ac) > PbS(Ac)–CdS(Ac). Lower times are detected when the acetate precursor is used, but results are not totally conclusive when the fitting error is considered, see Table 3. On the other hand, the fitting error for A_1, A_2 and A_3 is significantly lower compared to that for τ_1 and τ_2, allowing a more conclusive analysis of these data. It is worth noting that the weight of the

This journal is © the Owner Societies 2013

Phys. Chem. Chem. Phys., 2013, **00**, 1–9 | **5**

Table 3 Fitting parameters and corresponding errors of TG responses shown in Fig. 3(b) according to eqn (2). The weight of each decay process in percentage is also indicated

Sample	No. SILAR cycles (PbS–CdS)	τ_1 (ps)	τ_2 (ps)	A_1	A_2	A_3
PbS(N)	2/0	10 ± 1.3	182 ± 71	0.50 ± 0.03 54%	0.26 ± 0.03 28%	0.16 ± 0.03 18%
PbS(Ac)	1/0	8.7 ± 0.7	122 ± 15	0.44 ± 0.02 46%	0.29 ± 0.01 30%	0.23 ± 0.01 24%
PbS(N)–CdS(Ac)	2/5	6.50 ± 0.52	91 ± 6	0.26 ± 0.01 27%	0.22 ± 0.01 23%	0.49 ± 0.03 50%
PbS(Ac)–CdS(Ac)	1/5	4 ± 0.60	73 ± 12	0.17 ± 0.01 18%	0.09 ± 0.01 9%	0.71 ± 0.02 73%

three decay processes, A_1, A_2 and A_3, also changes systematically as shown in Table 3. A_1 and A_2 decrease as PbS(N) > PbS(Ac) > PbS(N)–CdS(Ac) > PbS(Ac)–CdS(Ac), while A_3 follows the opposite trend. One possible effect of the CdS coating on PbS is to reduce the surface defects of PbS QDs.[36] It is clear that the surface defects could greatly affect photoexcited electron and hole dynamics and concomitantly, the photovoltaic properties. In order to achieve high IPCE and photocurrents, surface defects should not be significantly reduced.[33] Therefore, the first two decay processes could be assigned to electron and hole trapping processes, and the last slow decay process corresponds to electron/hole injection. A_1 and A_2 correspond to trapped electron and hole concentration since these parameters significantly decrease after CdS coating, especially for PbS(Ac)–CdS(Ac). A_3 can be assigned to injection of electron/hole, i.e., the relative electron injection efficiency, dramatically increases after CdS coating. With this interpretation, compared to PbS(N), lower concentration of surface defects exist for PbS(Ac), from the different weight of the trapping/injection processes, see Table 3. These results are in good agreement with the J_{sc} values observed in Fig. 2(b). Therefore, we can conclude that the different weights observed in Table 3 can be attributed to different properties of the PbS surface states (nature, density, energy level…), with a dramatic impact on the photoinjection of carriers from PbS QDs. An increase of the injection efficiency is detected when Pb(Ac) is used as the precursor instead of Pb(N). In addition, after CdS deposition, the injection efficiency increases for both lead precursors, indicating that the CdS capping passivates the PbS surface states. A similar beneficial effect has been described for the ZnS capping used in QDSCs, which leads to a significant enhancement of the cell photocurrents.[19,47] Note that all the cells analyzed in Fig. 3 have also been capped with ZnS as described in the Experimental section.

In order to validate the conclusions extracted from the ultrafast characterization by the transient grating technique, surface photovoltage (SPV) measurements have been carried out. SPV is particularly sensitive to characterize charge separation.[48,49] It has been widely employed for the characterization of dye sensitized solar cells[42,50,51] and QDSCs.[52–54] In SPV, a voltage as a function of wavelength, for a modulated light beam, is recorded. In order to observe a SPV signal, two different processes must take place: (i) charge generation and (ii) charge separation.[48,49] Fig. 4 shows the typical modulated

SPV spectra obtained for the analyzed PbS–CdS samples, with the Ac precursor for both Pb and Cd deposition and 1 and 5 SILAR cycles, respectively. The modulated light beam is connected to a lock-in amplifier that measures the voltage originated from the charge separation of the photogenerated charge. Fig. 4 shows the in-phase and phase-shifted signals on linear and logarithmic scales. The in-phase signals were positive over the whole spectral range, providing evidence for preferential modulated separation of photo-generated electrons towards the internal interface.[42,48,50] On the linear scale, Fig 4(a), the onset of the SPV signals is located at approximately 1100 nm, due to the absorption in the PbS quantum dots and increased steeply at wavelengths below 550 nm and above 460 nm due to absorption in the CdS surface layer. On the logarithmic scale, Fig. 4(b), the absolute SPV signals can also be analyzed at the longer wavelengths. The noise level was about 100 nV for the given measurement conditions. The in-phase SPV signal reached the noise level at about 1300 nm and tended to increase slightly at longer wavelengths. In contrast, the phase-shifted by 90° SPV signal was above the noise level by
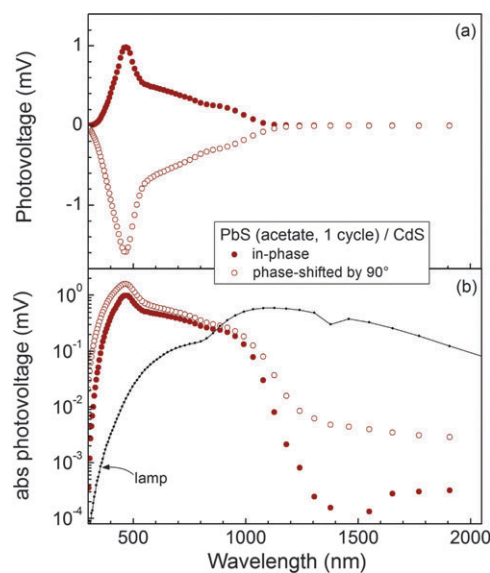

Fig. 4 Surface photovoltage spectra of the sample PbS(Ac)–CdS(Ac) with 1 and 5 cycles, respectively, for the in-phase (filled circles) and phase-shifted (open circles) SPV signals on (a) the linear scale and on (b) the logarithmic scale for the absolute signals. The line shows the intensity spectrum of the halogen lamp.
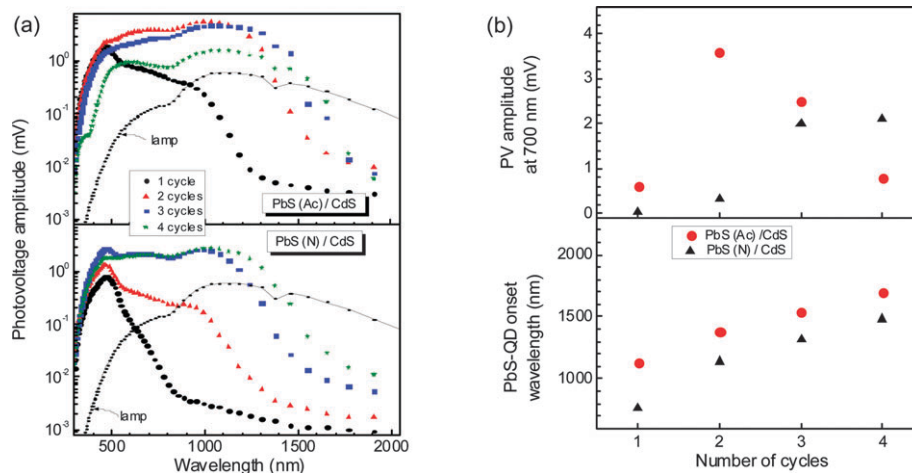
Fig. 5 (a) Spectra of the surface photovoltage amplitude of PbS(Ac)–CdS (on the top) and PbS(N)–CdS (below) samples for 1–4 cycles of PbS deposition by SILAR (circles, triangles, squares, and stars, respectively). 5 SILAR cycles and Cd(Ac) as the cadmium precursor have been used in all the cases for CdS deposition. The lines show the intensity spectrum of the halogen lamp. (b) Values of the surface photovoltage amplitude at 700 nm, (on the top) and of the wavelength related to the onset of the surface photovoltage due to absorption and charge separation in the PbS quantum dots (below) for the PbS (acetate)–CdS (circles) and PbS (nitrate)–CdS (triangles) as a function of the number of SILAR deposition cycles.

more than 20–30 times also at the longer wavelengths. Therefore, charge separation by excitation from electronic defect states below the excitonic band gap of the PbS quantum dots takes place while the disappearance of the in-phase signals gives evidence for a very slow relaxation within times much longer than the modulation period. Consequently, SPV measurements provide evidence of the presence of surface states.

The amplitude of the modulated SPV is defined as the square root of the sum of the squared in-phase and phase-shifted by 90° signals. The spectra of the SPV amplitude of PbS(Ac)–CdS(Ac) and PbS(N)–CdS(Ac) samples are plotted in Fig. 5(a) for 1–4 cycles of PbS deposition by SILAR. The SPV amplitude increased for 2 SILAR cycles compared to only 1 cycle for both types of samples while the increase was much more pronounced for the PbS(Ac) samples. The SPV amplitude decreased with further increase of the number of SILAR cycles for the PbS(Ac) samples but continued to increase for the PbS(N) samples. This behavior is reflected in Fig. 5(b) showing the dependence of the SPV amplitude at 700 nm as a function of the number of SILAR cycles. For the PbS(Ac) samples, the value of the SPV amplitude at 700 nm increased from 0.62 mV for 1 SILAR cycle to 3.63 mV for 2 SILAR cycles and decreased to 2.4 and 0.8 mV for 3 and 4 SILAR cycles, respectively. For the PbS(N) samples the value of the SPV amplitude at 700 nm increased from 0.034 mV for 1 SILAR cycles to 0.32, 2.0 and 2.1 mV for 2–4 SILAR cycles, respectively. Therefore the highest modulated SPV amplitudes were reached for PbS(Ac) samples with a small number of SILAR cycles.

The wavelength onset due to the absorption in the PbS quantum dots shifted towards longer wavelength with increasing number of SILAR cycles which gives evidence for a systematic growth of PbS quantum dots with increasing effective layer thickness of PbS. The onset wavelengths are plotted in Fig. 5(b) as a function of the number of SILAR cycles. The onset wavelengths are determined as the wavelength where the SPV signal is one order

of magnitude lower than the maximum SPV signal. This is also easy to obtain graphically from the SPV plot on a linear scale, see S5 (ESI†). The onset wavelength for the PbS(Ac) samples increased from 1130 nm for 1 SILAR cycle to 1380, 1540 and 1700 nm for 2–4 SILAR cycles, respectively. For the PbS(N) samples the onset wavelengths were shorter compared to the PbS(Ac) samples and increased from 760 nm for 1 SILAR cycle to 1140, 1320 and 1480 nm for 2–4 SILAR cycles, respectively. It can be concluded that the effective SILAR deposition rate was higher for PbS(Ac), in good agreement with light absorption measurements, Fig 1(d).

Samples PbS(Ac) with 3 cycles and PbS(N) with 4 cycles can be properly compared with respect to the onset wavelengths and SPV amplitudes. The SPV amplitudes of these samples were 4.5 and 2.7 mV in the maximum and 0.007 and 0.011 mV at 1900 nm, respectively. Therefore, normalizing both signals at their maximum amplitudes, the SPV signals related to modulated charge separation from defect states at 1900 nm were more pronounced by a factor of 2.5 for the nitrate sample compared to the acetate one. This analysis indicates a high presence of traps at the band gap for nitrate samples, in good agreement with the results derived from TG characterization. The presence of trap states in the characterized samples and the higher density of traps for PbS (N) are also discussed in terms of the SPV phase in S6 (ESI†).

Conclusions

PbS–CdS QDSCs with reproducible conversion efficiencies higher than 4% have been fabricated using Pb and Cd acetate precursors in the SILAR QD growth processes. Unprecedented photocurrents for sensitized solar cells, including dye sensitized, higher than 20 mA cm^{-2} have been obtained. Compared to nitrate precursors, the use of acetate precursors leads to faster deposition rates of both PbS and CdS. We have shown

This journal is © the Owner Societies 2013

Phys. Chem. Chem. Phys., 2013, **00**, 1–9 | **7**

that besides this effect, the precursor plays a more intricate role in the final solar cell performance. Cells prepared with the same amount of light absorbing material exhibit higher performance when acetate precursors are employed. From impedance spectroscopy characterization, we ruled out any effect of the metallic precursor on the position of the TiO_2 conduction band and on the recombination rate of electrons in the TiO_2 for accepting species in QDs and/or the electrolyte. TG measurements indicate a stronger weight of injection in comparison with trapping in surface states for samples prepared with acetate precursors. SPV measurements have confirmed that the metallic precursor employed in the QD growth of PbS and CdS has a dramatic effect on the density of surface states. A lower density of traps is detected when the acetate precursor is employed for electrode sensitization. The exact mechanism to explain the different density of surface states caused by the different precursors is being currently investigated. This work unambiguously unveils the dramatic role that surface states play in the QDSC performance and paves the way for further improving the QDSC efficiencies by the appropriate treatment of surface states.

Acknowledgements

References

1 B. O'Regan and M. Grätzel, *Nature*, 1991, **353**, 737–740.
2 A. Yella, H.-W. Lee, H. N. Tsao, C. Yi, A. K. Chandiran, M. K. Nazeeruddin, E. W.-G. Diau, C.-Y. Yeh, S. M. Zakeeruddin and M. Grätzel, *Science*, 2011, **334**, 629–634.
3 F. Hetsch, X. Xu, H. Wang, S. V. Kershaw and A. L. Rogach, *J. Phys. Chem. Lett.*, 2011, **2**, 1879–1887.
4 G. Hodes, *J. Phys. Chem. C*, 2008, **112**, 17778–17787.
5 P. V. Kamat, *J. Phys. Chem. C*, 2008, **112**, 18737–18753.
6 P. V. Kamat, K. Tvrdy, D. R. Baker and J. G. Radich, *Chem. Rev.*, 2010, **110**, 6664–6688.
7 I. Mora-Seró and J. Bisquert, *J. Phys. Chem. Lett.*, 2010, **1**, 3046–3052.
8 S. Rühle, M. Shalom and A. Zaban, *ChemPhysChem*, 2010, **11**, 2290–2304.
9 Z. Yang, C.-Y. Chen, P. Roy and H.-T. Chang, *Chem. Commun.*, 2011, **47**, 9561–9571.
10 W. Yu, L. H. Qu, W. Z. Guo and X. G. Peng, *Chem. Mater.*, 2003, **15**, 2854–2860.
11 A. P. Alivisatos, *Science*, 1996, **271**, 933–937.
12 R. Vogel, P. Hoyer and H. Weller, *J. Phys. Chem.*, 1994, **98**, 3183–3188.
13 H.-S. Kim, C.-R. Lee, J.-H. Im, K.-B. Lee, T. Moehl, A. Marchioro, S.-J. Moon, R. Humphry-Baker, J.-H. Yum, J. E. Moser, M. Gratzel and N.-G. Park, *Sci. Rep.*, 2012, **2**. Q7
14 M. M. Lee, J. Teuscher, T. Miyasaka, T. N. Murakami and H. J. Snaith, *Science*, 2012, **338**, 643–647.
15 S. Giménez, X. Xu, T. Lana-Villarreal, R. Gómez, S. Agouram, Muñoz-Sanjosé and I. Mora-Seró, *J. Appl. Phys.*, 2010, Q8 **108**, 064310.
16 M. Samadpour, S. Giménez, P. P. Boix, Q. Shen, M. E. Calvo, N. Taghavinia, A. I. zad, T. Toyoda, H. Míguez and I. Mora-Seró, *Electrochim. Acta*, 2012, **75**, 139–147.
17 N. Guijarro, T. Lana-Villarreal, I. Mora-Seró, J. Bisquert and R. Gómez, *J. Phys. Chem. C*, 2009, **113**, 4208–4214.
18 I. Mora-Seró, S. Giménez, F. Fabregat-Santiago, R. Gómez, Q. Shen, T. Toyoda and J. Bisquert, *Acc. Chem. Res.*, 2009, **42**, 1848–1857.
19 S. Giménez, I. Mora-Seró, L. Macor, N. Guijarro, T. Lana-Villarreal, R. Gómez, L. J. Diguna, Q. Shen, T. Toyoda and J. Bisquert, *Nanotechnology*, 2009, **20**, 295204.
20 D. F. Watson, *J. Phys. Chem. Lett.*, 2010, **1**, 2299–2309.
21 I. Robel, V. Subramanian, M. Kuno and P. V. Kamat, *J. Am. Chem. Soc.*, 2006, **128**, 2385–2393.
22 Z. Pan, H. Zhang, K. Cheng, Y. Hou, J. Hua and X. Zhong, *ACS Nano*, 2012, **6**, 3982–3991.
23 Q. Shen, J. Kobayashi, L. J. Diguna and T. Toyoda, *J. Appl. Phys.*, 2008, **103**, 084304.
24 S. H. Im, C.-S. Lim, J. A. Chang, Y. H. Lee, N. Maiti, H.-J. Kim, M. K. Nazeeruddin, M. Grätzel and S. I. Seok, *Nano Lett.*, 2011, **11**, 4789–4793.
25 Q. Zhang, X. Guo, X. Huang, S. Huang, D. Li, Y. Luo, Q. Shen, T. Toyoda and Q. Meng, *Phys. Chem. Chem. Phys.*, 2011, **13**, 4659–4667.
26 H. J. Lee, M. Wang, P. Chen, D. R. Gamelin, S. M. Zakeeruddin, M. Grätzel and M. K. Nazeeruddin, *Nano Lett.*, 2009, **9**, 4221–4227.
27 P. K. Santra and P. V. Kamat, *J. Am. Chem. Soc.*, 2012, **134**, 2508–2511.
28 V. Gónzalez-Pedro, X. Xu, I. Mora-Seró and J. Bisquert, *ACS Nano*, 2010, **4**, 5783–5790.
29 C. Ratanatawanate, C. Xiong and K. J. Balkus, *ACS Nano*, 2008, **2**, 1682–1688.
30 S. M. Sze, *Physics of Semiconductor Devices*, John Wiley and Sons, New York, 1981.
31 B.-R. Hyun, Y.-W. Zhong, A. C. Bartnik, L. Sun, H. D. Abruña, F. W. Wise, J. D. Goodreau, J. R. Matthews, T. M. Leslie and N. F. Borrelli, *ACS Nano*, 2008, **2**, 2206–2212.
32 J. M. Luther, M. Law, M. C. Beard, Q. Song, M. O. Reese, R. J. Ellingson and A. J. Nozik, *Nano Lett.*, 2008, **8**, 3488–3492.
33 A. H. Ip, S. M. Thon, S. Hoogland, O. Voznyy, D. Zhitomirsky, R. Debnath, L. Levina, L. R. Rollny, G. H. Carey, A. Fischer, K. W. Kemp, I. J. Kramer, Z. Ning, A. J. Labelle, K. W. Chou,

8 | *Phys. Chem. Chem. Phys.*, 2013, **00**, 1–9

This journal is © the Owner Societies 2013

1 A. Amassian and E. H. Sargent, *Nat. Nanotechnol.*, 2012, **7**, 577–582.

34 H. J. Lee, H. C. Leventis, S.-J. Moon, P. Chen, S. Ito, S. A. Haque, T. Torres, F. Nüesch, T. Geiger, S. M. Zakeeruddin, M. Grätzel and M. K. Nazeeruddin, *Adv. Funct. Mater.*, 2009, **19**, 2735–2742.

35 M. Samadpour, P. P. Boix, S. Giménez, A. I. Zad, N. Taghavinia, I. Mora-Seró and J. Bisquert, *J. Phys. Chem. C*, 2011, **115**, 14400–14407.

36 A. Braga, S. Giménez, I. Concina, A. Vomiero and I. Mora-Seró, *J. Phys. Chem. Lett.*, 2011, **2**, 454–460.

37 M. A. Hossain, Z. Y. Koh and Q. Wang, *Phys. Chem. Chem. Phys.*, 2012, **14**, 7367–7374.

38 N. Zhou, G. Chen, X. Zhang, L. Cheng, Y. Luo, D. Li and Q. Meng, *Electrochem. Commun.*, 2012, **20**, 97–100.

39 G. Hodes, J. Manassen and D. Cahen, *J. Electrochem. Soc.*, 1980, **127**, 544–549.

40 Q. Shen, K. Katayama, M. Yamaguchi, T. Sawada and T. Toyoda, *Thin Solid Films*, 2005, **486**, 15–19.

41 Q. Shen, K. Katayama, T. Sawada, M. Yamaguchi and T. Toyoda, *Jpn. J. Appl. Phys.*, 2006, **45**, 5569–5574.

42 V. Duzhko, V. Y. Timoshenko, F. Koch and T. Dittrich, *Phys. Rev. B: Condens. Matter Mater. Phys.*, 2001, **64**, 75204.

43 M. A. Hossain, J. R. Jennings, C. Shen, J. H. Pan, Z. Y. Koh, N. Mathews and Q. Wang, *J. Mater. Chem.*, 2012, **22**, 16235–16242.

44 F. Fabregat-Santiago, G. Garcia-Belmonte, I. Mora-Seró and J. Bisquert, *Phys. Chem. Chem. Phys.*, 2011, **13**, 9083–9118.

45 Hod, V. González-Pedro, Z. Tachan, F. Fabregat-Santiago, I. Mora-Seró, J. Bisquert and A. Zaban, *J. Phys. Chem. Lett.*, 2011, **2**, 3032–3035.

46 H. Preier, *Appl. Phys.*, 1979, **20**, 189–206.

47 N. Guijarro, J. M. Campiña, Q. Shen, T. Toyoda, T. Lana-Villarreal and R. Gómez, *Phys. Chem. Chem. Phys.*, 2011, **13**, 12024–12032.

48 L. Kronik and Y. Shapira, *Surf. Interface Anal.*, 2001, **31**, 954.

49 I. Mora-Seró, T. Dittrich, G. Garcia-Belmonte and J. Bisquert, *J. Appl. Phys.*, 2006, **100**, 103705.

50 T. Dittrich, I. Mora-Seró, G. Garcia-Belmonte and J. Bisquert, *Phys. Rev. B: Condens. Matter Mater. Phys.*, 2006, **73**, 045407.

51 I. Mora-Seró, T. Dittrich, A. Belaidi, G. Garcia-Belmonte and J. Bisquert, *J. Phys. Chem. B*, 2005, **109**, 14932–14938.

52 I. Mora-Seró, J. Bisquert, T. Dittrich, A. Belaidi, A. S. Susha and A. L. Rogach, *J. Phys. Chem. C*, 2007, **111**, 14889–14892.

53 I. Mora-Seró, T. Dittrich, A. S. Susha, A. L. Rogach and J. Bisquert, *Thin Solid Films*, 2008, **516**, 6994–6998.

54 I. Mora-Seró, D. Gross, T. Mittereder, A. A. Lutich, A. Susha, T. Dittrich, A. Belaidi, R. Caballero, F. Langa, J. Bisquert and A. L. Rogach, *Small*, 2010, **6**, 221–225.

This journal is © the Owner Societies 2013

Phys. Chem. Chem. Phys., 2013, **00**, 1–9 | **9**